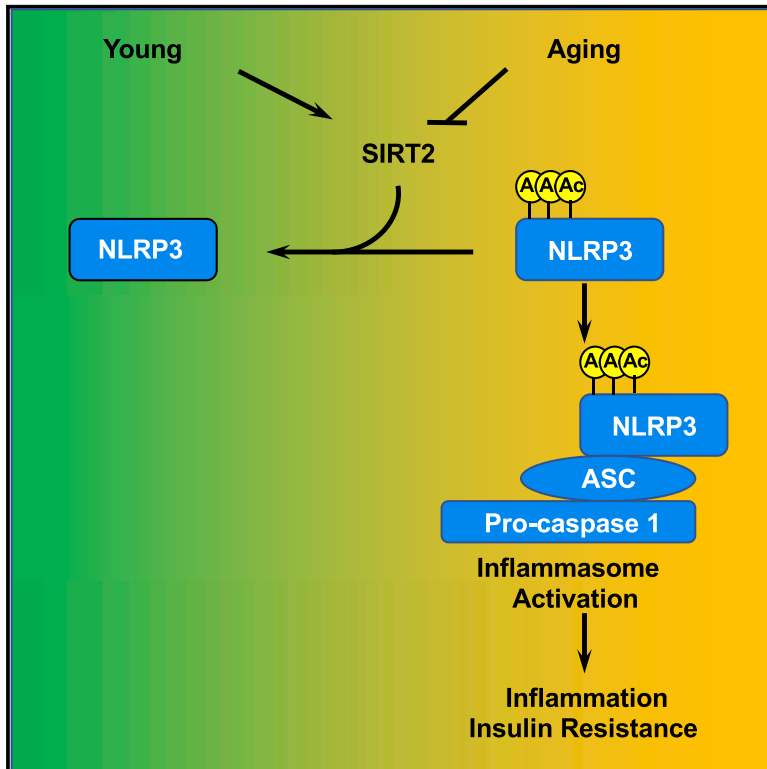


# Cell Metabolism

## An Acetylation Switch of the NLRP3 Inflammasome Regulates Aging-Associated Chronic Inflammation and Insulin Resistance

### Graphical Abstract



### Authors

Ming He, Hou-Hsien Chiang, Hanzhi Luo, ..., Shimin Zhao, Hao Wu, Danica Chen

### Correspondence

danicac@berkeley.edu

### In Brief

He et al. show that SIRT2 deacetylates NLRP3 and inactivates the NLRP3 inflammasome. This interplay prevents, and can be targeted to reverse, aging-associated inflammation and insulin resistance. This study uncovers a mechanism underlying inflammaging and highlights the reversibility of aging-associated conditions.

### Highlights

- NLRP3 is modified by acetylation and deacetylated by SIRT2
- NLRP3 acetylation facilitates the activation of the NLRP3 inflammasome
- SIRT2 prevents and reverses aging-associated inflammation and insulin resistance
- NLRP3 deacetylation regulates aging-associated inflammation and insulin resistance

# An Acetylation Switch of the NLRP3 Inflammasome Regulates Aging-Associated Chronic Inflammation and Insulin Resistance

Ming He,<sup>1,5,8</sup> Hou-Hsien Chiang,<sup>1,6,8</sup> Hanzhi Luo,<sup>1,7,8</sup> Zhifang Zheng,<sup>1,8</sup> Qi Qiao,<sup>2,3</sup> Li Wang,<sup>2,3</sup> Mingdian Tan,<sup>1</sup> Rika Ohkubo,<sup>1</sup> Wei-Chieh Mu,<sup>1</sup> Shimin Zhao,<sup>4</sup> Hao Wu,<sup>2,3</sup> and Danica Chen<sup>1,9,\*</sup>

<sup>1</sup>Program in Metabolic Biology, Nutritional Sciences & Toxicology, University of California, Berkeley, CA 94720, USA

<sup>2</sup>Department of Biological Chemistry and Molecular Pharmacology, Harvard Medical School, Boston, MA 02115, USA

<sup>3</sup>Program in Cellular and Molecular Medicine, Boston Children's Hospital, Boston, MA 02115, USA

<sup>4</sup>School of Life Sciences, Fudan University, Shanghai, China

<sup>5</sup>Present address: Department of Pathophysiology, Key Laboratory of Cell Differentiation and Apoptosis of Chinese Ministry of Education, Shanghai Jiao Tong University School of Medicine (SJTU-SM), Shanghai 200025, China

<sup>6</sup>Present address: Department of Internal Medicine, University of California, Davis, Sacramento, CA 95817, USA

<sup>7</sup>Present address: Molecular Pharmacology Program, Center for Cell Engineering, Center for Stem Cell Biology, Center for Experimental Therapeutics, Center for Hematologic Malignancies, Memorial Sloan Kettering Cancer Center, New York, NY, USA

<sup>8</sup>These authors contributed equally

<sup>9</sup>Lead Contact

\*Correspondence: [danicac@berkeley.edu](mailto:danicac@berkeley.edu)

<https://doi.org/10.1016/j.cmet.2020.01.009>

## SUMMARY

It is well documented that the rate of aging can be slowed, but it remains unclear to which extent aging-associated conditions can be reversed. How the interface of immunity and metabolism impinges upon the diabetes pandemic is largely unknown. Here, we show that NLRP3, a pattern recognition receptor, is modified by acetylation in macrophages and is deacetylated by SIRT2, an NAD<sup>+</sup>-dependent deacetylase and a metabolic sensor. We have developed a cell-based system that models aging-associated inflammation, a defined co-culture system that simulates the effects of inflammatory milieu on insulin resistance in metabolic tissues during aging, and aging mouse models; and demonstrate that SIRT2 and NLRP3 deacetylation prevent, and can be targeted to reverse, aging-associated inflammation and insulin resistance. These results establish the dysregulation of the acetylation switch of the NLRP3 inflammasome as an origin of aging-associated chronic inflammation and highlight the reversibility of aging-associated chronic inflammation and insulin resistance.

## INTRODUCTION

Aging is a systematic degenerative process that was long perceived as passive wear and tear. However, compelling evidence favors the view that aging is a regulated process amenable for genetic and environmental manipulations resulting in lifespan and healthspan extension (Kenyon, 2010; López-Otín et al., 2013). Evidence is also emerging to suggest that aging-associated conditions may be reversed. Prominently, aging-associated stem cell deterioration and tissue degeneration have been shown to be reversed by genetic regulators (Brown et al., 2013; Leeman et al., 2018; Luo et al., 2019; Mohrin et al., 2015). The extent to which aging-associated conditions can be reversed is unknown but has profound implications for enhancing healthspan in the world with a growing aging population.

The immune system has evolved to launch robust yet acute responses necessary to effectively eliminate pathogens and safeguard tissue integrity. Chronic low-grade inflammation has no survival advantage to the host, yet epidemiological studies showed a marked increase in pro-inflammatory cytokines in aged (Chung et al., 2006; Fagiolo et al., 1993; Ferrucci et al., 2005; Forsey et al., 2003; Hager et al., 1994; Myśliwska et al., 1998) or obese individuals (Hotamisligil, 2010; Vandanmagsar et al., 2011). Numerous studies have suggested a connection between chronic inflammation and age- or overnutrition-related

### Context and Significance

It is well-documented that the rate of aging can be slowed, but it remains unclear to which extent aging-associated conditions can be reversed. Understanding the reversibility of aging-associated conditions has important implications in treating aging-related diseases. Here, researchers at the University of California, Berkeley discovered that the SIRT2 enzyme regulates the NLRP3 inflammasome, a cellular machinery that produces inflammatory cytokines and prevents inflammation and insulin resistance in aged but not young mice. The researchers demonstrated that SIRT2 and NLRP3 modulation can be targeted to reverse inflammation and insulin resistance in aged mice. These findings demonstrate an underlying cause of aging-associated inflammation and highlight the reversibility of aging-associated conditions.



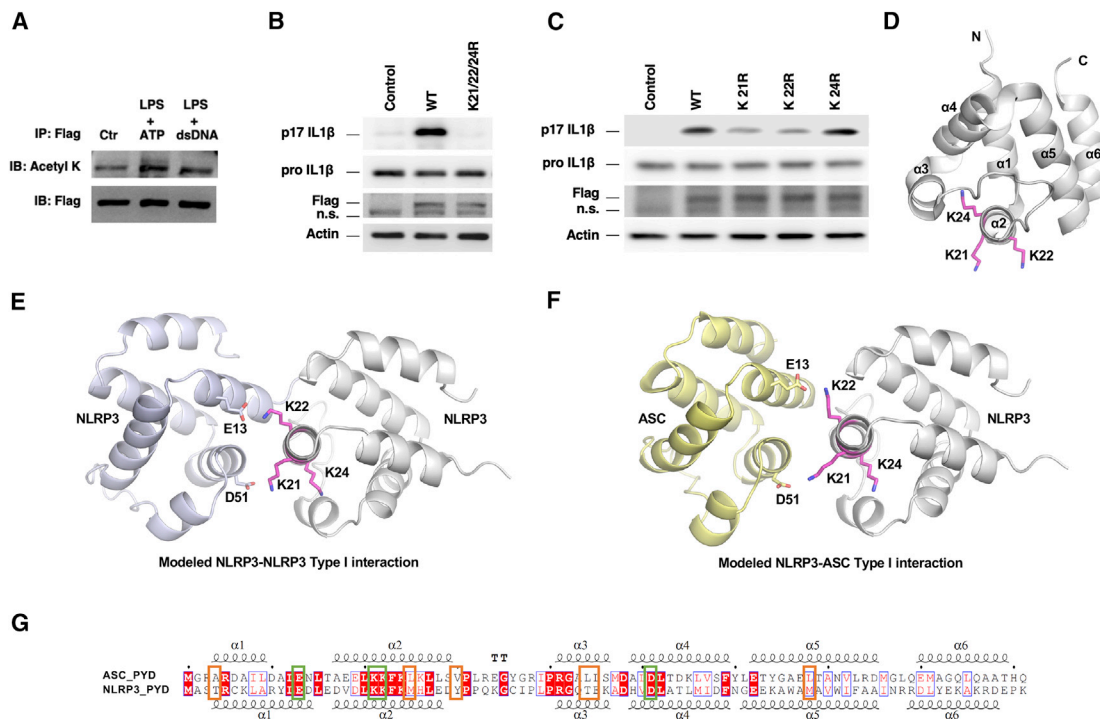


**Figure 2. Acetylation of NLRP3 Enhances the NLRP3 Inflammasome Assembly and Activity**

(A) NG5 cells were primed with LPS and treated with ATP or dsDNA. NLRP3-Flag was immunopurified followed by western analyses. (B and C) NLRP3 KO macrophages were reconstituted with NLRP3 mutants (B, NLRP3 mutant K21/22/24R; and C, NLRP3 mutants K21R, K22R, and K24R) and WT NLRP3 control by retroviral transduction and were stimulated with LPS and ATP. Cell lysates were used for western analyses for pro IL-1 $\beta$ . Culture supernatants were used for p17 IL-1 $\beta$  western analyses. n.s.: non-specific band. (D) Position of K21, K22, and K24 residues in NLRP3 PYD domain structure (PDB code: 2NAQ). (E and F) K21 and K22 are involved in Type I interactions in modeled NLRP3-NLRP3 interaction (E) and NLRP3-ASC interaction (F). (G) Sequence alignment of the PYD domain of NLRP3 and ASC indicates conserved charged residues (green box) and less conserved hydrophobic residues (orange box) in Type I interface. See also [Figure S2](#) and [Table S1](#).

S1A). Western analyses further confirmed that NLRP3 was modified by acetylation in macrophages (Figure 1C).

Sirtuins are NAD<sup>+</sup>-dependent deacetylases that regulate diverse metabolic processes (Du et al., 2011; Finkel et al., 2009; Jiang et al., 2011; Jing et al., 2016; Liu et al., 2008; Walker et al., 2010; Wang et al., 2010; Zhao et al., 2010). To determine whether sirtuins target NLRP3 for deacetylation, we knocked down sirtuins in NG5 cells via small interfering RNA (siRNA). Knocking down SIRT1 in NG5 cells did not have an effect on the acetylation level of NLRP3 (Figures S1B and S1C). In contrast, knocking down SIRT2 in NG5 cells increased the acetylation level of NLRP3 determined by western analyses (Figure 1D). These lysine residues targeted for acetylation are highly conserved in mammals (Figure 1E). Mutating these lysine residues reduced the acetylation levels of NLRP3 (Figure S1D). These results suggest that SIRT2 targets NLRP3 for deacetylation in macrophages.

Because SIRT2 deacetylates NLRP3, we investigated whether SIRT2 regulates the NLRP3 inflammasome activation. We isolated bone-marrow-derived macrophages (BMDMs) from wild-type (WT) and SIRT2 KO mice and stimulated the cells for inflammasome activation. The expression of pro-IL1 $\beta$  in stimulated WT and SIRT2 KO macrophages was comparable (Figure 1F). SIRT2 KO macrophages had increased production of IL-1 $\beta$  and

cleaved caspase 1 compared to WT controls in response to NLRP3 inducers such as nigericin and ATP (Figure 1F). However, there was no difference in IL-1 $\beta$  production and caspase 1 cleavage between WT and SIRT2 KO macrophages in response to flagellin, a NLRC4 inflammasome inducer, or dsDNA, an AIM2 inflammasome inducer (Figure 1F). Consistent with a role of SIRT2 in suppressing NLRP3 inflammasome activation, pharmacological inhibition of SIRT2 also enhances caspase 1 activation in response to NLRP3 induction (Misawa et al., 2013). Together, these results suggest that SIRT2 represses the NLRP3 inflammasome activity.

### Acetylation of NLRP3 Facilitates the Assembly and Activation of the NLRP3 Inflammasome

To investigate whether acetylation regulates the activity of the NLRP3 inflammasome, we treated NG5 cells with inducers for inflammasomes. Upon priming with lipopolysaccharides (LPS) followed by ATP stimulation to activate the NLRP3 inflammasome, the acetylation level of NLRP3 was increased (Figure 2A). However, treatment with LPS and dsDNA, an AIM2 inflammasome inducer, did not change the level of NLRP3 acetylation. The PYD domain mediates the interaction between NLRP3 and apoptosis-associated speck-like protein containing a CARD

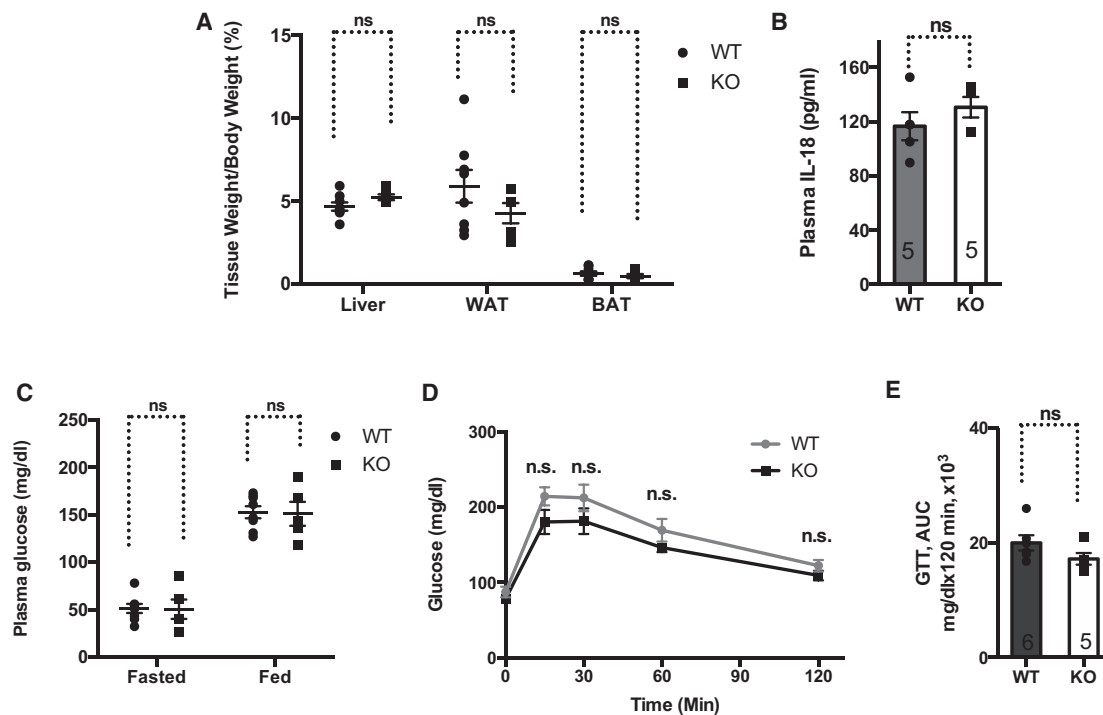


**Figure 3. Young SIRT2 KO Mice Fed a Chow Diet Are Metabolically Normal**

Young WT and SIRT2 KO mice fed a chow diet for 6 months were compared.

(A) Tissue weight.

(B) Plasma IL-18.

(C) Plasma glucose.

(D and E) Glucose tolerance test. (E) is the area under the curve for (D).

Error bars represent SE. n.s.:  $p > 0.05$ . Student's *t* test. See also [Figure S3](#).

(ASC), and the formation of the inflammasome (Lu et al., 2014). We mutated the lysine residues at the acetylation sites of NLRP3 to arginine to mimic the constitutively deacetylated state and reconstituted NLRP3 KO macrophages with WT or mutant NLRP3 (K21/22/24R) via retroviral transduction. WT and mutant NLRP3 were expressed to comparable levels (Figure 2B). Upon treatment with LPS and ATP, cells reconstituted with WT NLRP3 processed IL-1 $\beta$  (Figure 2B). In contrast, cells reconstituted with NLRP3 mutant had significantly reduced levels of IL-1 $\beta$  cleavage (Figure 2B). NLRP3 complexes with ASC to form inflammasome (Martinon et al., 2009; Strowig et al., 2012). In contrast to WT NLRP3, which triggered the formation of speck-like foci containing ASC, NLRP3 mutant was compromised in forming speck-like foci with ASC (Figures S2A and S2B), indicating that acetylation of NLRP3 facilitates the assembly and activation of the NLRP3 inflammasome.

We next made and tested single mutations of lysine residues to arginine. K21R and K22R mutants, but not K24R mutant, resulted in reduced NLRP3 inflammasome activation and compromised formation of speck-like foci with ASC (Figures 2C and S2C), consistent with the model that K21 and K22 mediate the PYD-PYD interaction (Lu et al., 2014). Structural analyses showed that K24 was partially buried in the interior of the PYD, while K21 and K22 pointed to the exterior of the domain (Figure 2D). There was sufficient space surrounding K24 to accommodate an R mutation in the structure, consistent with the lack

of effect of K24R mutant on inflammasome activity (Figure 2C). Similarly, the space was sufficient to accommodate an acetyl group, supporting a minimal effect from acetylation on K24.

The PYD interactions between NLRP3 and ASC, or ASC and ASC, or NLRP3 and NLRP3 use similar binding interfaces that are observed in the ASC filament structure (Lu et al., 2014; Oroz et al., 2016). To elucidate the potential structural mechanism for the effect of modification and mutation on K21 and K22, we modeled the NLRP3-NLRP3 and the NLRP3-ASC interactions by aligning the NLRP3 PYD structure (PDB code: 2NAQ) into the ASC oligomer (PDB code: 3J63) followed by energy minimization using the YASARA server (Krieger et al., 2009). K21 and K22 of NLRP3 were located at the Type I interface close to D51 and E13 of neighboring NLRP3 or ASC (Figures 2E and 2F), in keeping with disruption of charged interactions and impairment of ASC polymerization by K21E and K22E mutations (Lu et al., 2014). All these residues are conserved in the PYD domains of NLRP3 and ASC (Figure 2G, green box). Several hydrophobic residues in the PYD of ASC are also involved in oligomerization (Lu et al., 2014; Oroz et al., 2016), although they are less conserved in NLRP3 (Figure 2G, orange box). Collectively, the structural analyses suggest that acetylation at K21 and K22 of NLRP3 might alter both the charged interactions and the hydrophobic interactions.

To quantify the consequence of changing to arginine or acetyllysine (ALY) by acetylation at K21 and K22 of NLRP3, we modeled and energy-minimized six pairs of Type I PYD dimer

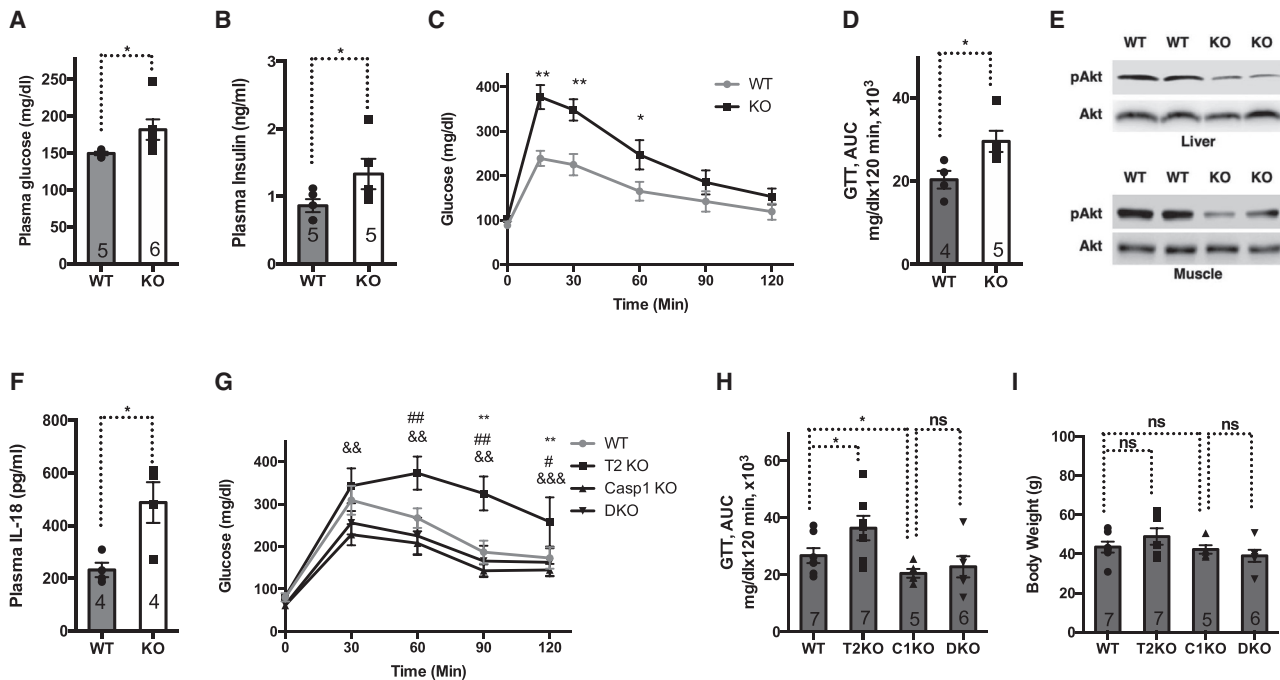


**Figure 4. SIRT2 Prevents Aging-Associated Chronic Inflammation and Insulin Resistance**

Two-year-old WT and SIRT2 KO mice fed a chow diet were compared.

(A) Plasma glucose.

(B) Plasma insulin.

(C) Glucose tolerance test.

(D) Area under the curve for (C).

(E) Western blots of AKT and phosphorylated AKT in the livers and muscles after the mice were infused with insulin.

(F) Plasma IL-18.

(G) Glucose tolerance test for aged WT, SIRT2 KO (T2 KO), caspase 1 KO (C1 KO), and SIRT2/caspase 1 double KO mice (DKO). Comparison of WT and SIRT2 KO marked with (\*). Comparison of WT and Caspase 1 KO marked with (#). Comparison of SIRT2 KO and DKO marked with (&).

(H) Area under the curve for (G).

(I) Body Weight for mice used in (G).

Error bars represent SE. (\*) and (#):  $p < 0.05$ . (\*\*), (##), and (&&):  $p < 0.01$ . (\*\*\*) and (&&&):  $p < 0.001$ . n.s.:  $p > 0.05$ . Student's *t* test and ANOVA. See also [Figure S4](#).

structures: WT NLRP3 or K21/22R or K21/22ALY in complex with WT NLRP3 or WT ASC. Structural analyses by PDBE/PISA ([http://www.ebi.ac.uk/msd-srv/prot\\_int/cgi-bin/piserver](http://www.ebi.ac.uk/msd-srv/prot_int/cgi-bin/piserver)) of the modeled complexes indicated that acetylation at K21 and K22 improved Type I interface stability through much enhanced hydrophobic interactions (Table S1). K21/22R mutations modestly enhanced the charged interactions but decreased overall interface stability due to loss of hydrophobic interactions. Furthermore, based on the energy calculation, acetylation and mutation at 21 and 22 positions of NLRP3 may affect the NLRP3-NLRP3 interaction more significantly than the NLRP3-ASC interaction (Table S1).

### SIRT2 Prevents Aging- and Overnutrition-Associated Chronic Inflammation and Insulin Resistance

We next determined the physiological relevance of SIRT2 regulation of the NLRP3 inflammasome by assessing the systematic inflammation and metabolic homeostasis of SIRT2 KO mice. Young SIRT2 KO mice were phenotypically unremarkable. Compared to the WT littermates, SIRT2 KO mice fed a chow diet for 6 months had normal body fat, similar levels of plasma IL-18 and glucose, and responded comparably in a glucose

tolerance test (Figure 3). Because the NLRP3 inflammasome can be activated by endogenous metabolic signals associated with obesity and aging (Wen et al., 2011; Youm et al., 2012), we characterized SIRT2 KO mice fed a high-fat diet for 6 months or fed a chow diet for 2 years. Compared to WT control mice, SIRT2 KO mice fed a high-fat diet accumulated more body fat (Figure S3A) and had increased levels of plasma glucose (Figure S3B) and insulin (Figure S3C). Glucose tolerance tests and insulin tolerance tests showed compromised glucose metabolism and insulin sensitivity in SIRT2 KO mice (Figures S3D–S3G), suggesting that SIRT2 prevents diet-induced obesity and insulin resistance. The plasma IL-18 level was increased in SIRT2 KO mice fed a high-fat diet compared to the WT controls (Figure S3H), consistent with increased activation of the NLRP3 inflammasome under the condition of diet-induced obesity in the absence of SIRT2. SIRT2 KO mice had increased infiltration of stromal vascular fraction cells and macrophages in the adipose tissue, as well as increased expression of inflammatory cytokines such as IL-6 (Figures S3I–S3K).

At 2 years old, SIRT2 KO mice fed a chow diet also exhibited increased levels of plasma glucose and insulin (Figures 4A and 4B). Aged SIRT2 KO mice could not clear glucose as effectively

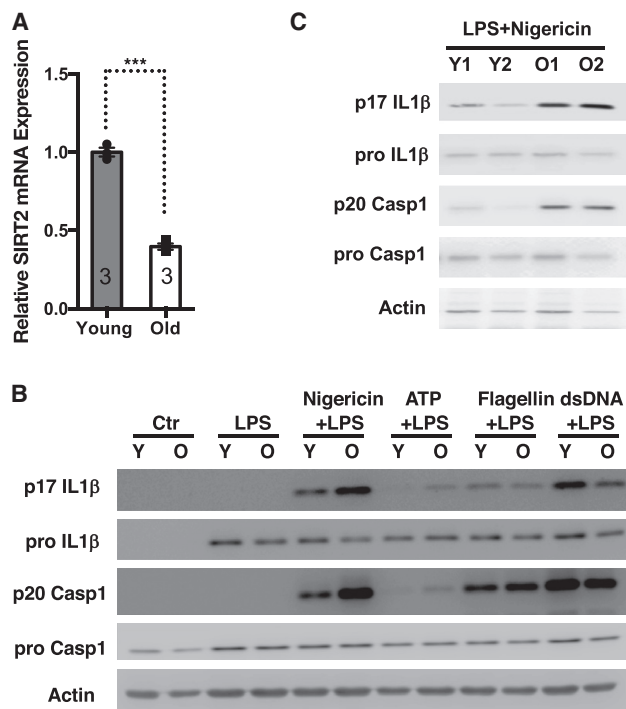


**Figure 5. A Cell-Based System that Models Aging-Associated Inflammation**

(A) SIRT2 mRNA levels in bone-marrow-derived macrophages (BMDMs) isolated from young and old mice were quantified by qPCR.

(B and C) BMDMs were isolated from young and old mice (B). Myeloid progenitors were isolated from bone marrow of young and old mice, immortalized with ER-Hoxb8, and differentiated into macrophages (C). Macrophages were primed with LPS and stimulated with nigericin, ATP, flagellin, or dsDNA. Cell lysates were used for western analyses for pro IL-1 $\beta$  and pro caspase 1. Culture supernatants were used for p17 IL-1 $\beta$  and p20 caspase 1 western analyses.

Error bars represent SE. \*\*\*p < 0.001. Student's t test.

as their WT control mice in glucose tolerance tests (Figures 4C and 4D) and showed impaired insulin signaling in insulin responsive tissues, as evidenced by reduced phosphorylation of Akt after the mice were infused with insulin (Figure 4E), indicating that SIRT2 is also required to maintain insulin sensitivity during physiological aging. Aged SIRT2 KO mice showed increased levels of plasma IL-18 (Figure 4F), suggesting that SIRT2 represses aging-associated NLRP3 inflammasome activation.

To assess whether the inflammation and glucose metabolism effects of SIRT2 is attributable to the hematopoietic origin, we reconstituted the hematopoietic system of lethally irradiated recipient mice with hematopoietic stem cells (HSCs) isolated from old WT and SIRT2 KO mice. Four months post-transplantation, mice reconstituted with SIRT2 KO HSCs had higher levels of plasma glucose, insulin, and IL-18 than mice reconstituted with WT HSCs (Figure S4). Thus, hematopoietic SIRT2 functions to repress aging-associated inflammation and maintains glucose homeostasis.

To determine whether SIRT2 maintains glucose homeostasis during physiological aging by repressing the NLRP3 inflammasome, we crossed SIRT2<sup>+/-</sup> and Caspase 1<sup>+/-</sup> to generate

SIRT2<sup>-/-</sup> Caspase 1<sup>-/-</sup>, aged them for 2 years, and performed glucose tolerance tests. While aged SIRT2<sup>-/-</sup> mice showed glucose intolerance compared to WT control mice, SIRT2<sup>-/-</sup> Caspase 1<sup>-/-</sup> mice and Caspase 1<sup>-/-</sup> mice had comparable glucose tolerance (Figures 4G and 4H). No body weight difference was noted due to either genetic manipulation (Figure 4I). Together, these data support a causal relationship between the inflammasome and SIRT2-mediated prevention of aging-related glucose intolerance.

### SIRT2 and NLRP3 Deacetylation Reverse Aging-Associated Inflammation and Insulin Resistance *Ex Vivo*

qPCR analyses of macrophages isolated from young (3 months old) and old mice (2 years old) showed that the expression of SIRT2 was decreased in old macrophages (Figure 5A). To test whether the NLRP3 inflammasome is activated in old macrophages, we stimulated BMDMs from young and old mice with inflammasome inducers. Old macrophages showed increased caspase 1 and IL-1 $\beta$  cleavage compared to young macrophages upon the stimulation with NLRP3 inducers (nigericin and ATP) but not NLRC4 (flagellin) or AIM2 inducer (dsDNA) (Figure 5B). Compared to young mice, plasma IL-18 level was increased in old mice (Figures 3B and 4F). Together, these data suggest that the NLRP3 inflammasome is specifically activated in macrophages during physiological aging and contributes to the increased inflammatory milieu.

We asked whether the SIRT2-NLRP3 axis can be targeted to reverse aging-associated inflammation. Primary macrophages are not amenable for long-term culture and genetic manipulation. To circumvent these limitations, we immortalized the myeloid progenitors isolated from young and old mice using ER-Hoxb8 retrovirus (Wang et al., 2006) before induction to differentiation. Macrophages derived from immortalized progenitors of old mice also showed higher NLRP3 activity than those of young mice (Figure 5C), indicating that this cell-based system derived from immortalized progenitors models NLRP3 activation in primary macrophages isolated from young and old mice. We infected immortalized progenitors of old mice with SIRT2 lentivirus and control virus, which was followed by induction to differentiation and inflammasome stimulation (Figure 6A). SIRT2 overexpression reduced the production of IL-1 $\beta$  and cleavage of caspase 1 in response to the stimulation with an NLRP3 inducer (ATP) but not an NLRC4 inducer (flagellin) in macrophages derived from old mice (Figure 6B). Furthermore, we tested the effects of NLRP3 acetylation on aging-associated NLRP3 activation. We transduced immortalized progenitors of old mice with WT or constitutively deacetylated mutant (K21/22/24R) NLRP3. Upon selection, differentiation, and inflammasome stimulation, old macrophages reconstituted with the constitutively deacetylated mutant NLRP3 showed decreased production of IL-1 $\beta$  and cleavage of caspase 1 (Figure 6C). These data suggest that SIRT2 inactivation and NLRP3 acetylation underlie aging-associated NLRP3 activation in macrophages and can be targeted to reverse aging-associated inflammation.

We sought to determine whether the SIRT2-NLRP3 axis can be targeted to reverse aging-associated insulin resistance. To this end, we took advantage of the cell-based system we established, which models NLRP3 activation in primary macrophages from young and old mice and devised a defined *in vitro*

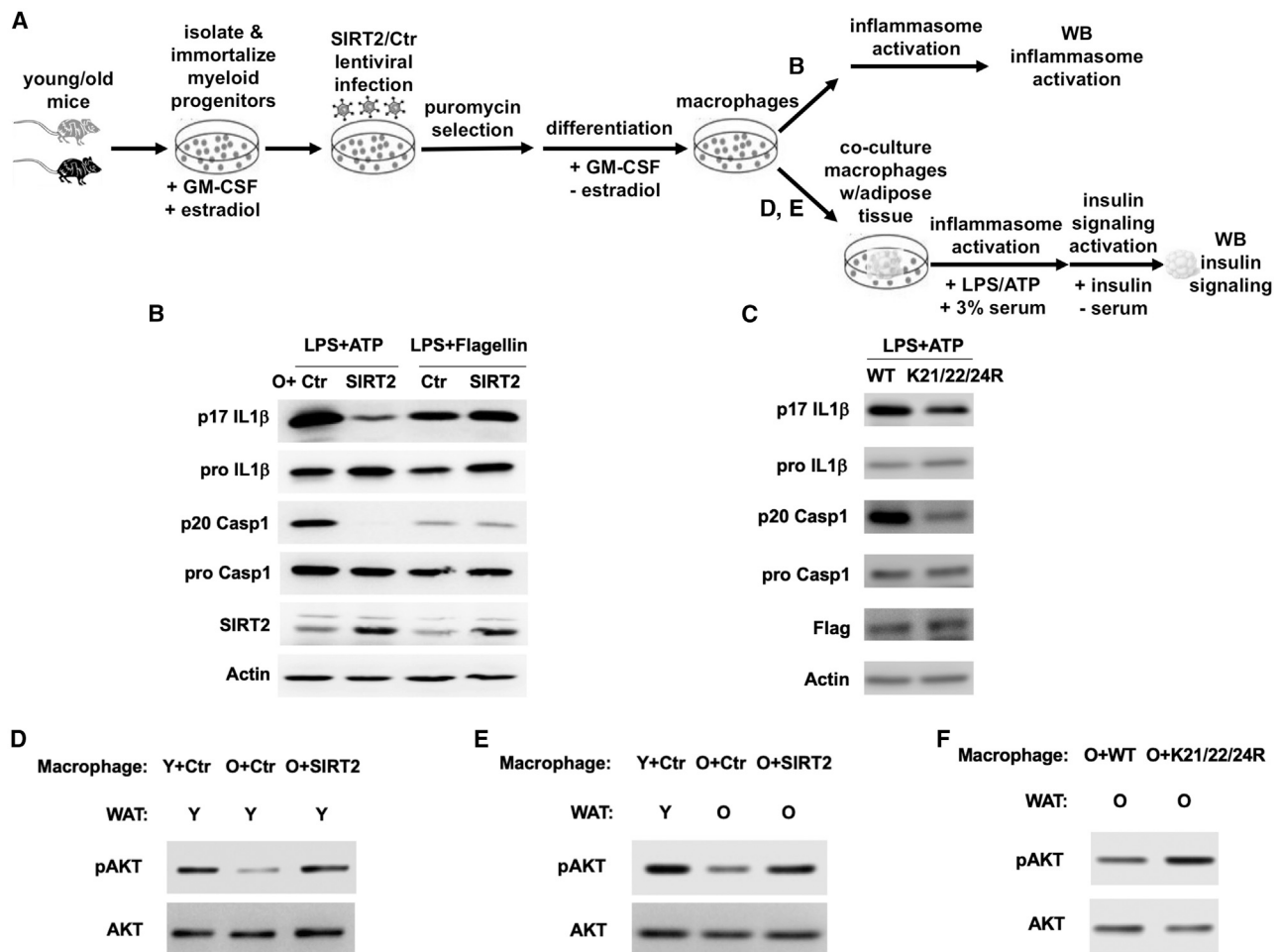


**Figure 6. SIRT2 and NLRP3 Deacetylation Reverse Aging-Associated Inflammation and Insulin Resistance**

(A) Experimental design.

(B and C) Immortalized myeloid progenitors from old WT mice were transduced with control or SIRT2 lentivirus (B), or WT or constitutively deacetylated mutant NLRP3 virus (C), selected, differentiated into macrophages, and treated for inflammasome activation. Cell lysates were used for western analyses for pro IL-1 $\beta$  and pro caspase 1. Culture supernatants were used for p17 IL-1 $\beta$  and p20 caspase 1 western analyses.

(D–F) Macrophages derived from immortalized myeloid progenitors from young or old mice with specified transduction were co-cultured with a piece of intact white adipose tissue from young or old mice as indicated and stimulated for NLRP3 inflammasome activation followed by insulin signaling activation. The insulin signaling in the white adipose tissues was assessed by western analyses. (D, effect of SIRT2 expression in old macrophages on insulin signaling in young white adipose tissues; E, effect of SIRT2 expression in old macrophages on insulin signaling in old white adipose tissues; and F, effect of NLRP3 acetylation in old macrophages on insulin signaling in old white adipose tissues).

co-culture system to simulate the effects of the inflammatory milieu derived from the NLRP3 inflammasome on insulin resistance in metabolic tissues (Figure 6A). We co-cultured the macrophages derived from the immortalized myeloid progenitors of young or old mice with a piece of intact white adipose tissue from young or old mice and induced NLRP3 inflammasome activation followed by insulin signaling activation, before the white adipose tissues were analyzed for insulin signaling by western analyses. We first compared the effect of overexpressing SIRT2 in old macrophages on white adipose tissues of young mice. Compared to young macrophages, co-culturing old macrophages with young white adipose tissues reduced insulin signaling, suggesting that the aberrant activation of the NLRP3 inflammasome in old macrophages is sufficient to induce insulin resistance in metabolic tissues (Figure 6D). Co-culturing old

macrophages overexpressing SIRT2 with young white adipose tissues enhanced insulin signaling (Figure 6D), consistent with a role of SIRT2 in repressing the NLRP3 inflammasome in old macrophages (Figure 6B).

We next co-cultured young macrophages with young white adipose tissues (simulating young animals), old macrophages with old white adipose tissues (simulating old animals), and old macrophages overexpressing SIRT2 with old white adipose tissues, which enabled us to assess whether SIRT2 activation in old macrophages can improve insulin resistance in old animals. We also co-cultured old macrophages transduced with WT or constitutively deacetylated mutant NLRP3 with old white adipose tissues to determine the effects of NLRP3 acetylation in old macrophages on insulin resistance in old animals. Compared to co-culture of young macrophages with young

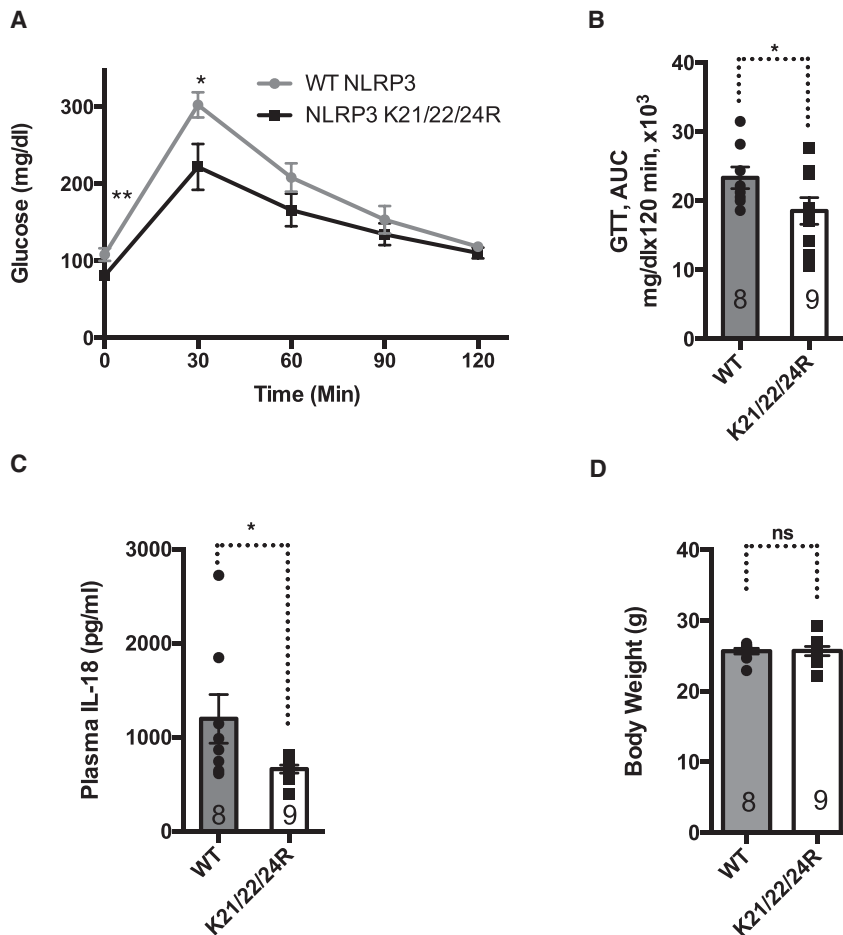


**Figure 7. NLRP3 Deacetylation Improves Aging-Associated Glucose Homeostasis *In Vivo***

Hematopoietic stem cells from aged WT mice were transduced with WT or K21/22/24R mutant NLRP3 and transplanted into lethally irradiated aged WT mice to reconstitute their hematopoietic system. Mice were analyzed 6 weeks post-transplantation for glucose tolerance tests (A and B), plasma IL-18 (C), and body weight (D). (B) is the area under the curve for (A). Error bars represent SE. \* $p < 0.05$ . n.s.:  $p > 0.05$ . Student's *t* test.

than the mice reconstituted with the hematopoietic system expressing WT NLRP3 (Figures 7A and 7B). Plasma level of IL-18 was lower in the aged mice reconstituted with the hematopoietic system expressing K21/22/24R mutant NLRP3 than the control mice expressing WT NLRP3 (Figure 7C), while there was no body weight difference between these two groups (Figure 7D). Together, these data suggest a functional role of NLRP3 acetylation in regulating aging-associated glucose homeostasis *in vivo*.

## DISCUSSION

Collectively, our work establishes a defined *in vitro* system that models aging-associated inflammation and insulin resistance and enables further studies for feasibility and mechanistic basis, as well as therapeutic

white adipose tissues, co-culture of old macrophages with old white adipose tissues resulted in reduced insulin signaling (Figure 6E). Overexpression of SIRT2 in old macrophages enhanced the insulin signaling in old white adipose tissues to the level comparable with young white adipose tissues co-cultured with young macrophages (Figure 6E). Compared to WT NLRP3, old macrophages reconstituted with constitutively deacetylated mutant NLRP3 (K21/22/24R) improved the insulin signaling in old white adipose tissues (Figure 6F). Thus, aging-associated insulin resistance can be reversed by quenching the inflammatory milieu, such as targeting the SIRT2-NLRP3 axis in macrophages.

### NLRP3 Deacetylation Improves Aging-Associated Glucose Homeostasis *In Vivo*

To determine whether the NLRP3 acetylation switch in macrophages regulates aging-associated glucose metabolism *in vivo*, we generated aged mouse models reconstituted with the hematopoietic system expressing WT or K21/22/24R mutant NLRP3. We transduced HSCs isolated from aged mice with WT or K21/22/24R mutant NLRP3 virus, which were transplanted into lethally irradiated aged mice. Six weeks post-transplantation, glucose tolerance tests showed that aged mice reconstituted with the hematopoietic system expressing K21/22/24R mutant NLRP3 cleared glucose more effectively

applications of reversing aging-associated inflammation and insulin resistance. Our studies identify an acetylation switch of the NLRP3 inflammasome in macrophages as a regulatory mechanism to ensure robust yet acute immune responses. Dysregulation of the acetylation switch of the NLRP3 inflammasome underlies chronic low-grade inflammation associated with aging and overnutrition and perpetuates the development of insulin resistance. Importantly, this regulatory mechanism can be targeted to reverse aging-associated inflammation and insulin resistance.

Dysregulation of the NLRP3 inflammasome is implicated in numerous pathological conditions (Duell et al., 2010; Guo et al., 2015; Heneka et al., 2013; Inoue et al., 2012; Jourdan et al., 2013; Yan et al., 2015). Its activity must be kept in check to prevent untoward physiological consequences and is subjected to multilayered regulation at the transcriptional (Bauernfeind et al., 2009) and posttranscriptional levels, such as phosphorylation (Song et al., 2017), ubiquitination (Py et al., 2013), and acetylation (Figure 1). The existence of the multilayered regulation may be essential to ensure an “on” or “off” switch for this powerful inflammatory machinery. We demonstrate that such fine regulation may be compromised under certain physiological conditions, such as aging and overnutrition (Figures 4, 6, 7, and S3).

Advances in sirtuin biology suggest that sirtuins can modify multiple proteins with related functions to exert a concerted

cellular function (Luo et al., 2017). Our new finding and a study by Misawa et al. (2013) indicate that SIRT2 regulates at least two downstream targets (NLRP3 and tubulin) to suppress two critical steps of the NLRP3 inflammasome activation (NLRP3 inflammasome assembly and transport) and suggest inactivation of the NLRP3 inflammasome is an important cellular function of SIRT2.

Sirtuins regulate a diverse array of cellular pathways and physiological events. Because sirtuins possess NAD<sup>+</sup>-dependent deacetylase activities, a number of histone and non-histone substrates for sirtuins have been identified (Finkel et al., 2009; Jiang et al., 2011; Liu et al., 2008; Qiu et al., 2010; Shin et al., 2011; Someya et al., 2010; Tao et al., 2010; Wang et al., 2010; Zhao et al., 2010). Although it is appreciated that acylation modulates protein biochemistry and regulates cellular functions, direct evidence supporting that acylation impacts physiological function is lacking. Using an *ex vivo* co-culture system (Figure 6) and an *in vivo* mouse model reconstituted with the hematopoietic system expressing a constitutively deacetylated mutant (Figure 7), we provide evidence that acetylation impacts an aspect of physiology.

Aging is associated with the accumulation of somatic mutations in the hematopoietic system and expansion of the mutated blood cells (Busque et al., 2012; Genovese et al., 2014; Jaiswal et al., 2014; McKerrell et al., 2015; Xie et al., 2014). Individuals with clonal hematopoiesis are at higher risk for not only blood diseases, but also diseases in distant tissues and earlier mortality (Bonfond et al., 2013; Goodell and Rando, 2015; Jaiswal et al., 2014). These observations support the notion that aging-associated defects in HSCs can be propagated in their progeny, thereby having detrimental effects on distant tissues and organismal healthspan (Goodell and Rando, 2015), and raise the question of the impact of HSC aging on the development of aging-related diseases (Chen and Kerr, 2019). HSC aging is regulated by a mitochondrial metabolic checkpoint that is monitored by the SIRT2-NLRP3 axis (Brown et al., 2013; Chen and Kerr, 2019; Luo et al., 2019; Mohrin and Chen, 2016; Mohrin et al., 2015). Mouse models reconstituted with SIRT2 KO HSCs exhibited aging-associated chronic inflammation and compromised glucose homeostasis (Figure S4), while animals reconstituted with mutant NLRP3 HSCs showed improved inflammation and glucose homeostasis (Figure 7). Our findings suggest that HSC aging contributes to aging-associated chronic inflammation and loss of glucose homeostasis.

### Limitations of Study

The effects of SIRT2 and NLRP3 acetylation on inflammation and glucose homeostasis were tested in C57BL/6 mouse strain only. It will be valuable to test these effects in other genetic backgrounds.

### STAR★METHODS

Detailed methods are provided in the online version of this paper and include the following:

- KEY RESOURCES TABLE
- LEAD CONTACT AND MATERIALS AVAILABILITY
- EXPERIMENTAL MODEL AND SUBJECT DETAILS
  - Mice

### METHOD DETAILS

- Cell Culture and RNAi
- Pyroptosome Formation
- Immunoprecipitations
- Mapping of Acetylation on Lysine Residues
- mRNA Analysis
- Isolation and immortalization of Myeloid Progenitors
- Lentiviral and Retroviral Transduction of Macrophages
- Co-culture of Macrophages and White Adipose Tissues
- ELISA Test
- Glucose Tolerance Test and Insulin Tolerance Test
- Transplantation Assays
- Retroviral Transduction of HSCs
- Structure Modeling and Analysis

### QUANTIFICATION AND STATISTICAL ANALYSIS

### DATA AND CODE AVAILABILITY

### SUPPLEMENTAL INFORMATION

Supplemental Information can be found online at <https://doi.org/10.1016/j.cmet.2020.01.009>.

### ACKNOWLEDGMENTS

We thank R. Vance and H. Mao for discussion; L. Kohlstaedt for mass spectrometry; B. Py, J. Yuan, and E. Alnemri for NG5 and NLRP3 KO macrophages, NLRP3, and ASC constructs; and M. Kamps for MSCV-HoxB8 construct. This work was supported by NIH grants R01DK 117481 (D.C.), R01DK101885 (D.C.), R01AG063404 (D.C.), R01AG 063389 (D.C.), DP1HD087988 (H.W.), and R01AI124491 (H.W.); National Institute of Food and Agriculture (D.C.); France-Berkeley Fund (D.C.); Glenn/AFAR Scholarship (H.L.); James C.Y. Soong Fellowship (H.-H.C. and W.-C.M.); Government Scholarship for Study Abroad (GSSA) from Taiwan (W.-C.M.); the ITO Scholarship (R.O.); and the Honjo International Scholarship (R.O.).

### AUTHOR CONTRIBUTIONS

D.C. conceived the study; M.H., H.L., W.-C.M., and R.O. characterized the phenotypes of mouse models and BMDMs; H.C., Z.Z., and M.T. performed biochemical experiments; Q.Q., L.W., and H.W. performed structural studies; H.L. established mouse models; H.L. and Z.Z. established *in vitro* cell-based system and performed the experiments; S.Z. advised tandem mass spectrometry; and D.C. wrote the manuscript with contributions from all authors.

### DECLARATION OF INTERESTS

The authors declare no competing interests.

Received: December 20, 2018

Revised: June 13, 2019

Accepted: January 13, 2020

Published: February 6, 2020

### REFERENCES

- Aggarwal, B.B., Shishodia, S., Sandur, S.K., Pandey, M.K., and Sethi, G. (2006). Inflammation and cancer: how hot is the link? *Biochem. Pharmacol.* 72, 1605–1621.
- Barbieri, M., Ferrucci, L., Ragno, E., Corsi, A., Bandinelli, S., Bonafè, M., Olivieri, F., Giovagnetti, S., Franceschi, C., Guralnik, J.M., and Paolisso, G. (2003). Chronic inflammation and the effect of IGF-I on muscle strength and power in older persons. *Am. J. Physiol. Endocrinol. Metab.* 284, E481–E487.
- Bauernfeind, F.G., Horvath, G., Stutz, A., Alnemri, E.S., MacDonald, K., Speert, D., Fernandes-Alnemri, T., Wu, J., Monks, B.G., Fitzgerald, K.A.,

- et al. (2009). Cutting edge: NF- $\kappa$ B activating pattern recognition and cytokine receptors license NLRP3 inflammasome activation by regulating NLRP3 expression. *J. Immunol.* *183*, 787–791.
- Beasley, L.E., Koster, A., Newman, A.B., Javaid, M.K., Ferrucci, L., Kritchevsky, S.B., Kuller, L.H., Pahor, M., Schaap, L.A., Visser, M., et al.; Health ABC study (2009). Inflammation and race and gender differences in computerized tomography-measured adipose depots. *Obesity (Silver Spring)* *17*, 1062–1069.
- Bobrowska, A., Donmez, G., Weiss, A., Guarente, L., and Bates, G. (2012). SIRT2 ablation has no effect on tubulin acetylation in brain, cholesterol biosynthesis or the progression of Huntington's disease phenotypes in vivo. *PLoS ONE* *7*, e34805.
- Bonnefond, A., Skrobek, B., Lobbens, S., Eury, E., Thuillier, D., Cauchi, S., Lantieri, O., Balkau, B., Riboli, E., Marre, M., et al. (2013). Association between large detectable clonal mosaicism and type 2 diabetes with vascular complications. *Nat. Genet.* *45*, 1040–1043.
- Brown, K., Xie, S., Qiu, X., Mohrin, M., Shin, J., Liu, Y., Zhang, D., Scadden, D.T., and Chen, D. (2013). SIRT3 reverses aging-associated degeneration. *Cell Rep.* *3*, 319–327.
- Busque, L., Patel, J.P., Figueroa, M.E., Vasanthakumar, A., Provost, S., Hamilou, Z., Mollica, L., Li, J., Viale, A., Heguy, A., et al. (2012). Recurrent somatic TET2 mutations in normal elderly individuals with clonal hematopoiesis. *Nat. Genet.* *44*, 1179–1181.
- Cartier, A., Côté, M., Lemieux, I., Pérusse, L., Tremblay, A., Bouchard, C., and Després, J.P. (2009). Age-related differences in inflammatory markers in men: contribution of visceral adiposity. *Metabolism* *58*, 1452–1458.
- Cesari, M., Penninx, B.W., Newman, A.B., Kritchevsky, S.B., Nicklas, B.J., Sutton-Tyrrell, K., Rubin, S.M., Ding, J., Simonsick, E.M., Harris, T.B., and Pahor, M. (2003). Inflammatory markers and onset of cardiovascular events: results from the Health ABC study. *Circulation* *108*, 2317–2322.
- Cesari, M., Penninx, B.W., Pahor, M., Lauretani, F., Corsi, A.M., Rhys Williams, G., Guralnik, J.M., and Ferrucci, L. (2004). Inflammatory markers and physical performance in older persons: the InCHIANTI study. *J. Gerontol. A Biol. Sci. Med. Sci.* *59*, 242–248.
- Chen, D., and Kerr, C. (2019). The Epigenetics of Stem Cell Aging Comes of Age. *Trends Cell Biol.* *29*, 563–568.
- Chung, H.Y., Sung, B., Jung, K.J., Zou, Y., and Yu, B.P. (2006). The molecular inflammatory process in aging. *Antioxid. Redox Signal.* *8*, 572–581.
- Cociorva, D., Tabb, D.L., and Yates, J.R. (2007). Validation of tandem mass spectrometry database search results using DTASelect. *Curr. Protoc. Bioinformatics* *76*, 13.4.1–13.4.14.
- Cushman, M., Arnold, A.M., Psaty, B.M., Manolio, T.A., Kuller, L.H., Burke, G.L., Polak, J.F., and Tracy, R.P. (2005). C-reactive protein and the 10-year incidence of coronary heart disease in older men and women: the cardiovascular health study. *Circulation* *112*, 25–31.
- Delano, W.L. (2002). The PyMol Molecular Graphics System, Version 1.3 (Schrödinger, LLC).
- Du, J., Zhou, Y., Su, X., Yu, J.J., Khan, S., Jiang, H., Kim, J., Woo, J., Kim, J.H., Choi, B.H., et al. (2011). Sirt5 is a NAD-dependent protein lysine demalonylase and desuccinylase. *Science* *334*, 806–809.
- Duewell, P., Kono, H., Rayner, K.J., Sirois, C.M., Vladimer, G., Bauernfeind, F.G., Abela, G.S., Franchi, L., Nuñez, G., Schnurr, M., et al. (2010). NLRP3 inflammasomes are required for atherogenesis and activated by cholesterol crystals. *Nature* *464*, 1357–1361.
- Emsley, P., and Cowtan, K. (2004). Coot: model-building tools for molecular graphics. *Acta Crystallogr. D Biol. Crystallogr.* *60*, 2126–2132.
- Fagiolo, U., Cossarizza, A., Scala, E., Fanale-Belasio, E., Ortolani, C., Cozzi, E., Monti, D., Franceschi, C., and Paganelli, R. (1993). Increased cytokine production in mononuclear cells of healthy elderly people. *Eur. J. Immunol.* *23*, 2375–2378.
- Fernandes-Alnemri, T., Yu, J.W., Datta, P., Wu, J., and Alnemri, E.S. (2009). AIM2 activates the inflammasome and cell death in response to cytoplasmic DNA. *Nature* *458*, 509–513.
- Ferrucci, L., Corsi, A., Lauretani, F., Bandinelli, S., Bartali, B., Taub, D.D., Guralnik, J.M., and Longo, D.L. (2005). The origins of age-related proinflammatory state. *Blood* *105*, 2294–2299.
- Finkel, T., Deng, C.X., and Mostoslavsky, R. (2009). Recent progress in the biology and physiology of sirtuins. *Nature* *460*, 587–591.
- Forsey, R.J., Thompson, J.M., Ernerudh, J., Hurst, T.L., Strindhall, J., Johansson, B., Nilsson, B.O., and Wikby, A. (2003). Plasma cytokine profiles in elderly humans. *Mech. Ageing Dev.* *124*, 487–493.
- Genovese, G., Kähler, A.K., Handsaker, R.E., Lindberg, J., Rose, S.A., Bakhoum, S.F., Chambert, K., Mick, E., Neale, B.M., Fromer, M., et al. (2014). Clonal hematopoiesis and blood-cancer risk inferred from blood DNA sequence. *N. Engl. J. Med.* *371*, 2477–2487.
- Goodell, M.A., and Rando, T.A. (2015). Stem cells and healthy aging. *Science* *350*, 1199–1204.
- Guo, H., Callaway, J.B., and Ting, J.P. (2015). Inflammasomes: mechanism of action, role in disease, and therapeutics. *Nat. Med.* *21*, 677–687.
- Hager, K., Machein, U., Krieger, S., Platt, D., Seefried, G., and Bauer, J. (1994). Interleukin-6 and selected plasma proteins in healthy persons of different ages. *Neurobiol. Aging* *15*, 771–772.
- Heneka, M.T., Kummer, M.P., Stutz, A., Delekate, A., Schwartz, S., Vieira-Saecker, A., Griep, A., Axt, D., Remus, A., Tzeng, T.C., et al. (2013). NLRP3 is activated in Alzheimer's disease and contributes to pathology in APP/PS1 mice. *Nature* *493*, 674–678.
- Hotamisligil, G.S. (2010). Endoplasmic reticulum stress and the inflammatory basis of metabolic disease. *Cell* *140*, 900–917.
- Hsu, F.C., Kritchevsky, S.B., Liu, Y., Kanaya, A., Newman, A.B., Perry, S.E., Visser, M., Pahor, M., Harris, T.B., and Nicklas, B.J.; Health ABC Study (2009). Association between inflammatory components and physical function in the health, aging, and body composition study: a principal component analysis approach. *J. Gerontol. A Biol. Sci. Med. Sci.* *64*, 581–589.
- Inoue, M., Williams, K.L., Gunn, M.D., and Shinohara, M.L. (2012). NLRP3 inflammasome induces chemotactic immune cell migration to the CNS in experimental autoimmune encephalomyelitis. *Proc. Natl. Acad. Sci. USA* *109*, 10480–10485.
- Jaiswal, S., Fontanillas, P., Flannick, J., Manning, A., Grauman, P.V., Mar, B.G., Lindley, R.C., Mermel, C.H., Burt, N., Chavez, A., et al. (2014). Age-related clonal hematopoiesis associated with adverse outcomes. *N. Engl. J. Med.* *371*, 2488–2498.
- Jiang, W., Wang, S., Xiao, M., Lin, Y., Zhou, L., Lei, Q., Xiong, Y., Guan, K.L., and Zhao, S. (2011). Acetylation regulates gluconeogenesis by promoting PEPCK1 degradation via recruiting the UBR5 ubiquitin ligase. *Mol. Cell* *43*, 33–44.
- Jing, H., Hu, J., He, B., Negrón Abril, Y.L., Stupinski, J., Weiser, K., Carbonaro, M., Chiang, Y.L., Southard, T., Giannakou, P., et al. (2016). A SIRT2-Selective Inhibitor Promotes c-Myc Oncoprotein Degradation and Exhibits Broad Anticancer Activity. *Cancer Cell* *29*, 297–310.
- Jourdan, T., Godlewski, G., Cinar, R., Bertola, A., Szanda, G., Liu, J., Tam, J., Han, T., Mukhopadhyay, B., Skarulis, M.C., et al. (2013). Activation of the Nlrp3 inflammasome in infiltrating macrophages by endocannabinoids mediates beta cell loss in type 2 diabetes. *Nat. Med.* *19*, 1132–1140.
- Kalogeropoulos, A., Georgiopoulou, V., Psaty, B.M., Rodondi, N., Smith, A.L., Harrison, D.G., Liu, Y., Hoffmann, U., Bauer, D.C., Newman, A.B., et al.; Health ABC Study Investigators (2010). Inflammatory markers and incident heart failure risk in older adults: the Health ABC (Health, Aging, and Body Composition) study. *J. Am. Coll. Cardiol.* *55*, 2129–2137.
- Kania, D.M., Binkley, N., Checovich, M., Havighurst, T., Schilling, M., and Ershler, W.B. (1995). Elevated plasma levels of interleukin-6 in postmenopausal women do not correlate with bone density. *J. Am. Geriatr. Soc.* *43*, 236–239.
- Kenyon, C.J. (2010). The genetics of ageing. *Nature* *464*, 504–512.
- Krieger, E., Joo, K., Lee, J., Lee, J., Raman, S., Thompson, J., Tyka, M., Baker, D., and Karplus, K. (2009). Improving physical realism, stereochemistry, and side-chain accuracy in homology modeling: Four approaches that performed well in CASP8. *Proteins* *77* (Suppl 9), 114–122.

- Krissinel, E., and Henrick, K. (2007). Inference of macromolecular assemblies from crystalline state. *J. Mol. Biol.* *372*, 774–797.
- Kuida, K., Lippke, J.A., Ku, G., Harding, M.W., Livingston, D.J., Su, M.S., and Flavell, R.A. (1995). Altered cytokine export and apoptosis in mice deficient in interleukin-1 beta converting enzyme. *Science* *267*, 2000–2003.
- Leeman, D.S., Hebestreit, K., Ruetz, T., Webb, A.E., McKay, A., Pollina, E.A., Dulken, B.W., Zhao, X., Yeo, R.W., Ho, T.T., et al. (2018). Lysosome activation clears aggregates and enhances quiescent neural stem cell activation during aging. *Science* *359*, 1277–1283.
- Liu, Y., Dentin, R., Chen, D., Hedrick, S., Ravnskjaer, K., Schenk, S., Milne, J., Meyers, D.J., Cole, P., Yates, J., 3rd, et al. (2008). A fasting inducible switch modulates gluconeogenesis via activator/coactivator exchange. *Nature* *456*, 269–273.
- López-Otín, C., Blasco, M.A., Partridge, L., Serrano, M., and Kroemer, G. (2013). The hallmarks of aging. *Cell* *153*, 1194–1217.
- Lu, M., Wan, M., Leavens, K.F., Chu, Q., Monks, B.R., Fernandez, S., Ahima, R.S., Ueki, K., Kahn, C.R., and Birnbaum, M.J. (2012). Insulin regulates liver metabolism in vivo in the absence of hepatic Akt and Foxo1. *Nat. Med.* *18*, 388–395.
- Lu, A., Magupalli, V.G., Ruan, J., Yin, Q., Atianand, M.K., Vos, M.R., Schröder, G.F., Fitzgerald, K.A., Wu, H., and Egelman, E.H. (2014). Unified polymerization mechanism for the assembly of ASC-dependent inflammasomes. *Cell* *156*, 1193–1206.
- Luo, H., Chiang, H.H., Louw, M., Susanto, A., and Chen, D. (2017). Nutrient Sensing and the Oxidative Stress Response. *Trends Endocrinol. Metab.* *28*, 449–460.
- Luo, H., Mu, W.C., Karki, R., Chiang, H.H., Mohrin, M., Shin, J.J., Ohkubo, R., Ito, K., Kanneganti, T.D., and Chen, D. (2019). Mitochondrial Stress-Initiated Aberrant Activation of the NLRP3 Inflammasome Regulates the Functional Deterioration of Hematopoietic Stem Cell Aging. *Cell. Rep.* *26*, 945–954.e4.
- Maggio, M., Basaria, S., Ceda, G.P., Ble, A., Ling, S.M., Bandinelli, S., Valentini, G., and Ferrucci, L. (2005). The relationship between testosterone and molecular markers of inflammation in older men. *J. Endocrinol. Invest.* *28* (11, Suppl Proceedings), 116–119.
- Maggio, M., Basaria, S., Ble, A., Lauretani, F., Bandinelli, S., Ceda, G.P., Valentini, G., Ling, S.M., and Ferrucci, L. (2006). Correlation between testosterone and the inflammatory marker soluble interleukin-6 receptor in older men. *J. Clin. Endocrinol. Metab.* *91*, 345–347.
- Martinon, F., Mayor, A., and Tschopp, J. (2009). The inflammasomes: guardians of the body. *Annu. Rev. Immunol.* *27*, 229–265.
- McDonald, W.H., Tabb, D.L., Sadygov, R.G., MacCoss, M.J., Venable, J., Graumann, J., Johnson, J.R., Cociorva, D., and Yates, J.R., 3rd (2004). MS1, MS2, and SQT-three unified, compact, and easily parsed file formats for the storage of shotgun proteomic spectra and identifications. *Rapid Commun. Mass Spectrom.* *18*, 2162–2168.
- McKerrell, T., Park, N., Moreno, T., Grove, C.S., Ponstingl, H., Stephens, J., Crawley, C., Craig, J., Scott, M.A., Hodgkinson, C., et al.; Understanding Society Scientific Group (2015). Leukemia-associated somatic mutations drive distinct patterns of age-related clonal hemopoiesis. *Cell Rep.* *10*, 1239–1245.
- Miao, H., Ou, J., Ma, Y., Guo, F., Yang, Z., Wiggins, M., Liu, C., Song, W., Han, X., Wang, M., et al. (2014). Macrophage CGI-58 deficiency activates ROS-inflammasome pathway to promote insulin resistance in mice. *Cell Rep.* *7*, 223–235.
- Misawa, T., Takahama, M., Kozaki, T., Lee, H., Zou, J., Saitoh, T., and Akira, S. (2013). Microtubule-driven spatial arrangement of mitochondria promotes activation of the NLRP3 inflammasome. *Nat. Immunol.* *14*, 454–460.
- Mohrin, M., and Chen, D. (2016). The mitochondrial metabolic checkpoint and aging of hematopoietic stem cells. *Curr. Opin. Hematol.* *23*, 318–324.
- Mohrin, M., Shin, J., Liu, Y., Brown, K., Luo, H., Xi, Y., Haynes, C.M., and Chen, D. (2015). Stem cell aging. A mitochondrial UPR-mediated metabolic checkpoint regulates hematopoietic stem cell aging. *Science* *347*, 1374–1377.
- Myśliwska, J., Bryl, E., Foerster, J., and Myśliwski, A. (1998). Increase of interleukin 6 and decrease of interleukin 2 production during the ageing process are influenced by the health status. *Mech. Ageing Dev.* *100*, 313–328.
- Oroz, J., Barrera-Vilarmau, S., Alfonso, C., Rivas, G., and de Alba, E. (2016). ASC Pyrin Domain Self-associates and Binds NLRP3 Protein Using Equivalent Binding Interfaces. *J. Biol. Chem.* *291*, 19487–19501.
- Park, S.K., Venable, J.D., Xu, T., and Yates, J.R., 3rd (2008). A quantitative analysis software tool for mass spectrometry-based proteomics. *Nat. Methods* *5*, 319–322.
- Peng, J., Elias, J.E., Thoreen, C.C., Licklider, L.J., and Gygi, S.P. (2003). Evaluation of multidimensional chromatography coupled with tandem mass spectrometry (LC/LC-MS/MS) for large-scale protein analysis: the yeast proteome. *J. Proteome Res.* *2*, 43–50.
- Pfeilschifter, J., Köditz, R., Pfohl, M., and Schatz, H. (2002). Changes in proinflammatory cytokine activity after menopause. *Endocr. Rev.* *23*, 90–119.
- Pickup, J.C., Chusney, G.D., Thomas, S.M., and Burt, D. (2000). Plasma interleukin-6, tumour necrosis factor alpha and blood cytokine production in type 2 diabetes. *Life Sci.* *67*, 291–300.
- Place, D.E., and Kanneganti, T.D. (2018). Recent advances in inflammasome biology. *Curr. Opin. Immunol.* *50*, 32–38.
- Pou, K.M., Massaro, J.M., Hoffmann, U., Vasan, R.S., Maurovich-Horvat, P., Larson, M.G., Keaney, J.F., Jr., Meigs, J.B., Lipinska, I., Kathiresan, S., et al. (2007). Visceral and subcutaneous adipose tissue volumes are cross-sectionally related to markers of inflammation and oxidative stress: the Framingham Heart Study. *Circulation* *116*, 1234–1241.
- Pradhan, A.D., Manson, J.E., Rifai, N., Buring, J.E., and Ridker, P.M. (2001). C-reactive protein, interleukin 6, and risk of developing type 2 diabetes mellitus. *JAMA* *286*, 327–334.
- Py, B.F., Kim, M.S., Vakifahmetoglu-Norberg, H., and Yuan, J. (2013). Deubiquitination of NLRP3 by BRCC3 critically regulates inflammasome activity. *Mol. Cell* *49*, 331–338.
- Qiu, X., Brown, K., Hirschev, M.D., Verdin, E., and Chen, D. (2010). Calorie restriction reduces oxidative stress by SIRT3-mediated SOD2 activation. *Cell Metab.* *12*, 662–667.
- Ravaglia, G., Forti, P., Maioli, F., Chiappelli, M., Montesi, F., Tumini, E., Mariani, E., Licastro, F., and Patterson, C. (2007). Blood inflammatory markers and risk of dementia: The ConSelice Study of Brain Aging. *Neurobiol. Aging* *28*, 1810–1820.
- Rodondi, N., Marques-Vidal, P., Butler, J., Sutton-Tyrrell, K., Cornuz, J., Satterfield, S., Harris, T., Bauer, D.C., Ferrucci, L., Vittinghoff, E., and Newman, A.B.; Health, Aging, and Body Composition Study (2010). Markers of atherosclerosis and inflammation for prediction of coronary heart disease in older adults. *Am. J. Epidemiol.* *171*, 540–549.
- Schaap, L.A., Pluijm, S.M., Deeg, D.J., Harris, T.B., Kritchevsky, S.B., Newman, A.B., Colbert, L.H., Pahor, M., Rubin, S.M., Tylavsky, F.A., and Visser, M.; Health ABC Study (2009). Higher inflammatory marker levels in older persons: associations with 5-year change in muscle mass and muscle strength. *J. Gerontol. A Biol. Sci. Med. Sci.* *64*, 1183–1189.
- Shin, J., Zhang, D., and Chen, D. (2011). Reversible acetylation of metabolic enzymes celebration: SIRT2 and p300 join the party. *Mol. Cell* *43*, 3–5.
- Shin, J., He, M., Liu, Y., Paredes, S., Villanova, L., Brown, K., Qiu, X., Nabavi, N., Mohrin, M., Wojnoonski, K., et al. (2013). SIRT7 represses Myc activity to suppress ER stress and prevent fatty liver disease. *Cell Rep.* *5*, 654–665.
- Someya, S., Yu, W., Hallows, W.C., Xu, J., Vann, J.M., Leeuwenburgh, C., Tanokura, M., Denu, J.M., and Prolla, T.A. (2010). Sirt3 mediates reduction of oxidative damage and prevention of age-related hearing loss under caloric restriction. *Cell* *143*, 802–812.
- Song, N., Liu, Z.S., Xue, W., Bai, Z.F., Wang, Q.Y., Dai, J., Liu, X., Huang, Y.J., Cai, H., Zhan, X.Y., et al. (2017). NLRP3 Phosphorylation Is an Essential Priming Event for Inflammasome Activation. *Mol. Cell* *68*, 185–197.e6.
- Strowig, T., Henao-Mejia, J., Elinav, E., and Flavell, R. (2012). Inflammasomes in health and disease. *Nature* *481*, 278–286.
- Tabb, D.L., McDonald, W.H., and Yates, J.R., 3rd (2002). DTASelect and Contrast: tools for assembling and comparing protein identifications from shotgun proteomics. *J. Proteome Res.* *1*, 21–26.
- Tao, R., Coleman, M.C., Pennington, J.D., Ozden, O., Park, S.H., Jiang, H., Kim, H.S., Flynn, C.R., Hill, S., Hayes McDonald, W., et al. (2010). Sirt3-

- mediated deacetylation of evolutionarily conserved lysine 122 regulates MnSOD activity in response to stress. *Mol. Cell* **40**, 893–904.
- Tracy, R.P., Lemaitre, R.N., Psaty, B.M., Ives, D.G., Evans, R.W., Cushman, M., Meilahn, E.N., and Kuller, L.H. (1997). Relationship of C-reactive protein to risk of cardiovascular disease in the elderly. Results from the Cardiovascular Health Study and the Rural Health Promotion Project. *Arterioscler. Thromb. Vasc. Biol.* **17**, 1121–1127.
- Vandanmagsar, B., Youm, Y.H., Ravussin, A., Galgani, J.E., Stadler, K., Mynatt, R.L., Ravussin, E., Stephens, J.M., and Dixit, V.D. (2011). The NLRP3 inflammasome instigates obesity-induced inflammation and insulin resistance. *Nat. Med.* **17**, 179–188.
- Walker, A.K., Yang, F., Jiang, K., Ji, J.Y., Watts, J.L., Purushotham, A., Boss, O., Hirsch, M.L., Ribich, S., Smith, J.J., et al. (2010). Conserved role of SIRT1 orthologs in fasting-dependent inhibition of the lipid/cholesterol regulator SREBP. *Genes Dev.* **24**, 1403–1417.
- Wang, G.G., Calvo, K.R., Pasillas, M.P., Sykes, D.B., Häcker, H., and Kamps, M.P. (2006). Quantitative production of macrophages or neutrophils ex vivo using conditional Hoxb8. *Nat. Methods* **3**, 287–293.
- Wang, Q., Zhang, Y., Yang, C., Xiong, H., Lin, Y., Yao, J., Li, H., Xie, L., Zhao, W., Yao, Y., et al. (2010). Acetylation of metabolic enzymes coordinates carbon source utilization and metabolic flux. *Science* **327**, 1004–1007.
- Washburn, M.P., Wolters, D., and Yates, J.R., 3rd (2001). Large-scale analysis of the yeast proteome by multidimensional protein identification technology. *Nat. Biotechnol.* **19**, 242–247.
- Weaver, J.D., Huang, M.H., Albert, M., Harris, T., Rowe, J.W., and Seeman, T.E. (2002). Interleukin-6 and risk of cognitive decline: MacArthur studies of successful aging. *Neurology* **59**, 371–378.
- Wen, H., Gris, D., Lei, Y., Jha, S., Zhang, L., Huang, M.T., Brickey, W.J., and Ting, J.P. (2011). Fatty acid-induced NLRP3-ASC inflammasome activation interferes with insulin signaling. *Nat. Immunol.* **12**, 408–415.
- Xie, M., Lu, C., Wang, J., McLellan, M.D., Johnson, K.J., Wendl, M.C., McMichael, J.F., Schmidt, H.K., Yellapantula, V., Miller, C.A., et al. (2014). Age-related mutations associated with clonal hematopoietic expansion and malignancies. *Nat. Med.* **20**, 1472–1478.
- Xu, T., Park, S.K., Venable, J.D., Wohlschlegel, J.A., Diedrich, J.K., Cociorva, D., Lu, B., Liao, L., Hewel, J., Han, X., et al. (2015). ProLuCID: An improved SEQUEST-like algorithm with enhanced sensitivity and specificity. *J. Proteomics* **129**, 16–24.
- Yaffe, K., Lindquist, K., Penninx, B.W., Simonsick, E.M., Pahor, M., Kritchevsky, S., Launer, L., Kuller, L., Rubin, S., and Harris, T. (2003). Inflammatory markers and cognition in well-functioning African-American and white elders. *Neurology* **61**, 76–80.
- Yan, Y., Jiang, W., Liu, L., Wang, X., Ding, C., Tian, Z., and Zhou, R. (2015). Dopamine controls systemic inflammation through inhibition of NLRP3 inflammasome. *Cell* **160**, 62–73.
- Youm, Y.H., Kanneganti, T.D., Vandanmagsar, B., Zhu, X., Ravussin, A., Adijiang, A., Owen, J.S., Thomas, M.J., Francis, J., Parks, J.S., and Dixit, V.D. (2012). The Nlrp3 inflammasome promotes age-related thymic demise and immunosenescence. *Cell Rep.* **1**, 56–68.
- Zhao, C., Chen, A., Jamieson, C.H., Fereshteh, M., Abrahamsson, A., Blum, J., Kwon, H.Y., Kim, J., Chute, J.P., Rizzieri, D., et al. (2009). Hedgehog signalling is essential for maintenance of cancer stem cells in myeloid leukaemia. *Nature* **458**, 776–779.
- Zhao, S., Xu, W., Jiang, W., Yu, W., Lin, Y., Zhang, T., Yao, J., Zhou, L., Zeng, Y., Li, H., et al. (2010). Regulation of cellular metabolism by protein lysine acetylation. *Science* **327**, 1000–1004.

## STAR★METHODS

### KEY RESOURCES TABLE

REAGENT or RESOURCE	SOURCE	IDENTIFIER
<b>Antibodies</b>		
Anti-Actin antibody produced in rabbit	Sigma-Aldrich	Cat# A2066; RRID: AB_476693
Caspase 1 Monoclonal Antibody (5B10), eBioscience(TM)	Thermo Fisher Scientific	Cat# 14-9832; RRID: AB_2016691
SIRT2 antibody	Santa Cruz	Cat# SC 20966; RRID: AB_2188598
SIRT2 antibody	Proteintech	Cat# 15345-1-AP
Monoclonal ANTI-FLAG antibody	Sigma-Aldrich	Cat# F1804, RRID:AB_262044
rabbit IgG antibody	Santa Cruz	Cat# sc-2027, RRID:AB_737197
GAPDH Antibody	Santa Cruz	Cat# sc-25778, RRID:AB_10167668
anti-Acetylated Lysine antibody	Biolegend	Cat# 623402, RRID:AB_315968
Caspase 1 Monoclonal Antibody	Thermo Fisher Scientific	Cat# 14-9832-80, RRID:AB_2016624
Mouse IL-1 beta/IL-1F2 Polyclonal antibody	R&D Systems	Cat# AF-401-NA, RRID:AB_416684
AKT antibody	Cell Signaling	Cat# 9272, RRID:AB_329827
Phospho-Akt (Ser473) antibody	Cell Signaling	Cat# 4060, RRID:AB_2315049
Streptavidin APC-Cy7	Biolegend	405208
CD3 Biotin	Biolegend	Cat# 100304; RRID: AB_312669
B220 Biotin	Biolegend	Cat# 103204; RRID: AB_312989
Gr1 Biotin	Biolegend	Cat# 108404; RRID: AB_313369
CD8a Biotin	Biolegend	Cat# 100704; RRID: AB_312743
Mac1 Biotin	Biolegend	Cat# 101204; RRID: AB_312787
Ter119 Biotin	Biolegend	Cat# 116204; RRID: AB_313705
CD4 Biotin	Biolegend	Cat# 100404; RRID: AB_312689
CD48 FITC	Biolegend	Cat# 103404; RRID: AB_313019
CD150 PE	Biolegend	Cat# 115904; RRID: AB_313683
c-Kit APC	Biolegend	Cat# 105812; RRID: AB_313221
Sca1 Pacific Blue	Biolegend	Cat# 108120; RRID: AB_493273
<b>Chemicals, Peptides, and Recombinant Proteins</b>		
LPS	Invivogen	Cat# tlr1-eklps
Nigericin	Sigma	Cat# N7143
ATP	Invivogen	Cat#tlr1-atpl
Flagellin	Invivogen	Cat#tlr1-epstfla
dsDNA	Invivogen	Cat# tlr1-patn
D-glucose	Sigma	Cat# G8270
Insulin	Sigma	Cat# I0516
Dulbecco's Modification of Eagle's Medium	Invitrogen	<b>Cat# 11965092</b>
Fetal Bovine Serum	Invitrogen	Cat#10437-028
Penicillin Streptomycin Solution (100x)	Invitrogen	<b>Cat# 15140122</b>
0.25% Trypsin	Invitrogen	<b>Cat# 25200056</b>
TRIZOL Reagent	Invitrogen	<b>Cat# 15596026</b>
RNAiMax	Invitrogen	<b>Cat# 13778150</b>
ANTI-FLAG® M2 Affinity Gel	Sigma	<b>Cat# A2220</b>
Protein A/G PLUS-Agarose	Santa Cruz	<b>Cat# sc-2003</b>
Protease inhibitor	Thermo	Cat# A32963
Lipofectamine 2000	Invitrogen	<b>Cat# 11668019</b>
trichloroacetic acid (TCA)	Sigma	Cat# T0699

(Continued on next page)

**Continued**

REAGENT or RESOURCE	SOURCE	IDENTIFIER
CD117 (c-kit) MicroBeads, mouse	Miltenyi Biotec	Cat# 130-094-224
Stemspan SFEM	Stemcell technologies	Cat# 09600
ES-Cult FBS	Stemcell technologies	Cat# 06952
Murine IL3	Peprotech	Cat# 213-13
Murine IL6	Peprotech	Cat# 216-16
Murine Flt3 ligand	Peprotech	Cat# 250-31L
Murine TPO	Peprotech	Cat# 315-14
Murine SCF	Peprotech	Cat# 250-03
Murine GM-CSF	Peprotech	Cat# 315-03
Estradiol	Sigma	E8875
Puromycin	Sigma	P9620
Ficoll-Paque plus	GE-healthcare Life Science	17144002
<b>Critical Commercial Assays</b>		
Mouse IL-18 ELISA Kit	MBL international	Cat#7625
Mouse Insulin ELISA Kit	Crystal Chem	Cat#90080
Eva qPCR SuperMix kit	BioChain Institute	Cat# K5052200
QuikChange Lightning Site-Directed Mutagenesis Kit	Agilent Technologies	Cat# 210518
<b>Experimental Models: Cell Lines</b>		
HEK293T	ATCC	CRL-3216
NLRP3 KO macrophages	( <a href="#">Py et al., 2013</a> )	N/A
NG5	( <a href="#">Py et al., 2013</a> )	N/A
<b>Experimental Models: Organisms/Strains</b>		
Mouse: SIRT2 KO	( <a href="#">Bobrowska et al., 2012</a> )	N/A
Mouse: Caspase1 KO	( <a href="#">Kuida et al., 1995</a> )	N/A
Mouse: C57BL/6J	National Institute on Aging	N/A
<b>Oligonucleotides</b>		
SIRT2 qPCR forward TGGGCTGGATGAAAGAGAA	Elim	N/A
SIRT2 qPCR reverse GGTCCACCTTGGAGAAGTCTG	Elim	N/A
SIRT1 qPCR forward GCAACAGCATCTTGCCTGAT	Elim	N/A
SIRT1 qPCR reverse GTGCTACTGGTCTCACTT	Elim	N/A
Actin qPCR forward GATCTGGCACCACACCTTCT	Elim	N/A
Actin qPCR reverse GGGGTGTGAAGGTCTCAAA	Elim	N/A
SIRT2 siRNA CCAGAATAAGGCATTTCTCTA	QIAGEN	N/A
SIRT1 siRNA AAGCGGCTTGAGGGTAATCAA	QIAGEN	N/A
<b>Recombinant DNA</b>		
pMSCVgfp-NLRP3	( <a href="#">Fernandes-Alnemri et al., 2009</a> )	N/A
pMSCV-ASC-EGFP	( <a href="#">Fernandes-Alnemri et al., 2009</a> )	N/A
pFUGw-SIRT2	( <a href="#">Luo et al., 2019</a> )	N/A
pMSCV-Hoxb8	( <a href="#">Wang et al., 2006</a> )	N/A
EcoPac	( <a href="#">Wang et al., 2006</a> )	N/A

(Continued on next page)

### Continued

REAGENT or RESOURCE	SOURCE	IDENTIFIER
Software and Algorithms		
Coot	(Emsley and Cowtan, 2004)	<a href="https://www2.mrc-lmb.cam.ac.uk/personal/pemsley/coot/">https://www2.mrc-lmb.cam.ac.uk/personal/pemsley/coot/</a>
YASARA energy minimization server	(Krieger et al., 2009)	<a href="http://www.yasara.org/minimizationserver.htm">http://www.yasara.org/minimizationserver.htm</a>
PDBePISA server	(Krissinel and Henrick, 2007)	<a href="http://www.ebi.ac.uk/msd-srv/prot_int/cgi-bin/piserver">http://www.ebi.ac.uk/msd-srv/prot_int/cgi-bin/piserver</a>
PyMOL Molecular Graphics System, Version 1.3 Schrödinger, LLC	(Delano, 2002)	<a href="https://pymol.org/2/">https://pymol.org/2/</a>

## LEAD CONTACT AND MATERIALS AVAILABILITY

NLRP3 mutant plasmids and immortalized myeloid progenitors from young and old mice were generated in this study and are available upon request. Please contact the Lead Contact, Danica Chen ([danicac@berkeley.edu](mailto:danicac@berkeley.edu)).

## EXPERIMENTAL MODEL AND SUBJECT DETAILS

### Mice

SIRT2 knockout mice and caspase 1 knockout mice on C57BL6 background have been described (Bobrowska et al., 2012; Kuida et al., 1995). For co-culture experiments and transplant experiments, wild type mice on C57BL6 background were provided by the National Institute on Aging. Male mice were used in the study. Ages of the mice are specified in the description of each experiment and included in the figure legends of the corresponding experiments. Young mice were 3-5 months old and aged mice were 2 years old. Mice were housed on a 12:12 h light:dark cycle at 25°C with *ad libitum* access to water and standard laboratory chow diet provided by LabDiet (0007688). The high-fat diet was provided by OpenSource Diets (D12079B). All animal procedures were in accordance with the animal care committee at the University of California, Berkeley. Health status checks were carried out by vets and euthanasia were performed if mice showed clinically apparent bleeding, or inability to move, eat or drink, or neurological/psychological changes, or clinically apparent spontaneous tumor formation, or mutilation. For insulin signaling, mice were fasted for 5 h, injected with either phosphate-buffered saline or insulin (Sigma) at 2 mU/g body weight for 15 min (Lu et al., 2012).

## METHOD DETAILS

### Cell Culture and RNAi

293T cells, NG5 cells (sex unknown), NLRP3 KO cells (sex unknown) were cultured in DMEM with 10% FBS at 37°C with 5% CO<sub>2</sub>. Double-stranded siRNAs were purchased from QIAGEN and were transfected into cells via RNAiMax (Invitrogen) according to manufacturer's instructions. Mouse SIRT2 siRNA targeting sequence is 5'-CCAGAATAAGGCATTTCTCTA-3'. Mouse SIRT1 siRNA targeting sequence is AAGCGGCTTGAGGGTAATCAA. The control siRNA is non-targeting control (QIAGEN). To induce caspase 1 activation, macrophages were primed with 100ng/mL LPS for 12 h and then stimulated with ATP (3 mM) for 30mins, Nigericin (1.5 μM) for 1 h, flagellin (0.5 μg/mL) for 1 h, poly(dA:dT) (0.5 μg/mL) for 1 h. Proteins from culture media were trichloroacetic acid (TCA) precipitated for Western analyses of p17 IL-1β and p20 caspase 1. Proteins from cell lysates were analyzed for pro IL-1β and pro caspase 1. For NLRP3 acetylation, cells were glucose starved for 6 h before immunoprecipitation.

### Pyroptosome Formation

Pyroptosome formation was performed as previously described (Fernandes-Alnemri et al., 2009). Briefly, 5x10<sup>5</sup> 293T cells were co-transfected with 0.8μg ASC-EGFP and 1.2 μg WT or mutant NLRP3 or control vector via Lipofectamine 2000 (Invitrogen). 48 h posttransfection, cells were observed under fluorescence microscope for foci formation.

### Immunoprecipitations

Immunoprecipitations were performed as previously described (Shin et al., 2013). Proteins were extracted in lysis buffer (50 mM Tris-Cl pH 7.5, 150 mM NaCl, 10% glycerol, 2 mM MgCl<sub>2</sub>, 1 mM DTT, 1% NP40, 1mM PMSF, and protease inhibitor). Protein extracts were subjected to centrifugation at 14,000 rpm for 10 min. Protein lysates were precleared with protein A/G beads (Santa Cruz Biotechnology) for 30 min before immunoprecipitation with Flag-resin (Sigma) overnight. Immunoprecipitates were extensively washed with lysis buffer and eluted with either Flag peptide (Sigma) for western analyses or 100mM Glycine solution (pH 3) for mass spectrometry analyses.

### Mapping of Acetylation on Lysine Residues

Mass spectrometry was performed by the Vincent J. Coates Proteomics/Mass Spectrometry Laboratory at UC Berkeley. Protein samples were cut with trypsin or trypsin and chymotrypsin. A nano LC column was packed in a 100  $\mu\text{m}$  inner diameter glass capillary with an emitter tip. The column consisted of 10 cm of Polaris c18 5  $\mu\text{m}$  packing material (Varian), followed by 4 cm of Partisphere 5 SCX (Whatman). The column was loaded by use of a pressure bomb and washed extensively with buffer A (see below). The column was then directly coupled to an electrospray ionization source mounted on a Thermo-Fisher LTQ XL linear ion trap mass spectrometer. An Agilent 1200 HPLC equipped with a split line so as to deliver a flow rate of 300 nL/min was used for chromatography. Peptides were eluted using a 4-step MudPIT procedure (Washburn et al., 2001). Buffer A was 5% acetonitrile/ 0.02% heptafluorobutyric acid (HBFA); buffer B was 80% acetonitrile/ 0.02% HBFA. Buffer C was 250 mM ammonium acetate/ 5% acetonitrile/ 0.02% HBFA; buffer D was same as buffer C, but with 500 mM ammonium acetate.

Protein identification was done with Integrated Proteomics Pipeline (IP2, Integrated Proteomics Applications, Inc. San Diego, CA) using ProLuCID/Sequest, DTASelect2 and Census (Cociorva et al., 2007; Park et al., 2008; Tabb et al., 2002; Xu et al., 2015). Tandem mass spectra were extracted into ms1 and ms2 files from raw files using RawExtractor (McDonald et al., 2004). Data was searched against the NCBI *Mus musculus* protein database supplemented with sequences of common contaminants, concatenated to a decoy database in which the sequence for each entry in the original database was reversed (Peng et al., 2003). LTQ data was searched with 3000.0 milli-amu precursor tolerance and the fragment ions were restricted to a 600.0 ppm tolerance. All searches were parallelized and searched on the VJC proteomics cluster. Search space included all fully tryptic or chymotryptic peptide candidates with no missed cleavage restrictions. Carbamidomethylation (+57.02146) of cysteine was considered a static modification. We required 1 peptide per protein and both tryptic termini or chymotryptic for each peptide identification. The ProLuCID search results were assembled and filtered using the DTASelect program (Cociorva et al., 2007; Tabb et al., 2002) with a peptide false discovery rate (FDR) of 0.001 for single peptides and a peptide FDR of 0.005 for additional peptides for the same protein. Under such filtering conditions, the estimated false discovery rate was always less than 1% for the datasets used.

### mRNA Analysis

RNA was isolated from cells using Trizol reagent (Invitrogen). cDNA was generated using the qScript cDNA SuperMix (Quanta Biosciences). Gene expression was determined by real time PCR using Eva qPCR SuperMix kit (BioChain Institute) on an ABI StepOnePlus system. All data were normalized to  $\beta$ -Actin expression. PCR primers used for real time PCR were SIRT2-forward: TGGGCTGGATGAAAGAGAA. SIRT2-reverse: GGTCCACCTTGGAGAAGTCTG. SIRT1-forward: GCAACAGCATCTTGCCTGAT. SIRT1-reverse: GTGCTACTGGTCTCACTT.  $\beta$ -Actin-forward: GATCTGGCACCACCTTCT.  $\beta$ -Actin-reverse: GGGGTGTTGAAGGTCTCAA.

### Isolation and immortalization of Myeloid Progenitors

Immortalization of myeloid progenitors was performed as described (Wang et al., 2006). Briefly, bone marrow was isolated from the femurs of mice after ammonium-chloride-potassium lysis of red blood cells and centrifugation onto a cushion of Ficoll-Paque. Ficoll-purified progenitors were infected with ER-Hoxb8 retrovirus and cultured in myeloid progenitor culture medium (RPMI-1640 with 10% FBS, 1% pen-strep-glutamine, 20 ng/mL GM-CSF, 30  $\mu\text{M}$  beta mercaptoethanol, and 1  $\mu\text{M}$  estrogen). Immortalized myeloid progenitors were selected by moving nonadherent progenitor cells every 3 days to a new culture well for 3 weeks. Differentiation to macrophages was performed by removal of estrogen from the culture medium.

### Lentiviral and Retroviral Transduction of Macrophages

SIRT2 was cloned into the pFUGw lentiviral construct using BamH1 and Age1 sites. Lentivirus was produced as described (Qiu et al., 2010), concentrated by centrifugation, and resuspended with culture medium described above for NLRP3 KO cells or macrophages derived from myeloid progenitor cells. NLRP3 mutant constructs were generated using pMSCVgfp retroviral construct expressing WT NLRP3 and QuikChange Lightning Site-Directed Mutagenesis Kit (Agilent Technology). Retrovirus was generated by transfecting 293T cells (ATCC) with pMSCVgfp retroviral constructs as well as VSV-G and gag/pol expression vectors using Lipofectamine 2000 transfection kit (Invitrogen). 48 h posttransfection, culture supernatant was filtered through 0.45- $\mu\text{m}$ -pore cellulose acetate filters, supplemented with 10  $\mu\text{g}/\text{mL}$  of polybrene, and was applied to macrophages. Cells were subjected to another cycle of infection on the next day.

### Co-culture of Macrophages and White Adipose Tissues

The protocol is modified from (Miao et al., 2014). Briefly, macrophages were differentiated from the immortalized myeloid progenitors. A piece of intact epididymal white adipose tissue isolated from a wild type mouse was put into a well, in which macrophages were pre-cultured. The co-culture system was treated with 100 ng/mL LPS for 24 h and then stimulated with 3 mM ATP for 30 mins, then stimulated with 100 nM insulin for 30 min. The white adipose tissues were analyzed by Western analyses.

### ELISA Test

IL-1 $\beta$  and IL-18 concentration were measured using the ELISA kits (MBL international). Insulin concentration was measured using the insulin ELISA kit (Crystal Chem).

### Glucose Tolerance Test and Insulin Tolerance Test

Glucose tolerance test was performed on mice fasted for 12 h by giving an intraperitoneal injection of D-glucose (1–2 g glucose/kg body weight, Sigma). Insulin tolerance test was performed on fasted mice by giving an intraperitoneal injection of insulin (0.5U insulin/kg body weight, Sigma). Glucose concentrations were measured with a glucometer (Bayer Contour) at the indicated time points.

### Transplantation Assays

250 sorted hematopoietic stem cells from donor mice were mixed with helper bone marrow cells and injected into lethally irradiated recipient mice. A split lethal dose of irradiation of 900 rad (500 rad + 400 rad) was used to irradiate the recipient mice. The source of the helper bone marrow cells was the same as the recipient mice. Recipient mice were analyzed for glucose metabolism and inflammation.

### Retroviral Transduction of HSCs

As previously described (Zhao et al., 2009), sorted HSCs were prestimulated for 5–10 h in a 96 well U bottom dish in StemSpan SFEM (Stem Cell Technologies) supplemented with 10% FBS (Stem Cell Technologies), 1% Penicillin/Streptomycin (Invitrogen), IL3 (20ng/mL), IL6 (20ng/mL), TPO (50ng/mL), Flt3L (50ng/mL), and SCF (100ng/mL) (Peprotech). Retrovirus was produced as described above, concentrated by centrifugation, and resuspended with supplemented StemSpan SFEM media. The retroviral media were added to HSCs in a 96 well plate, spinoculated for 90 min at 270 g in the presence of 8ug/mL polybrene. This process was repeated 24 h later with a fresh batch of retroviral media.

### Structure Modeling and Analysis

Structure modeling was performed using existing NLRP3 PYD monomer structure (PDB code: 2NAQ) (Oroz et al., 2016) and ASC PYD filament structure (PDB code: 3J63) (Lu et al., 2014). NLRP3 PYD structure was aligned to one or two ASC molecules in the filament structure by Coot (Emsley and Cowtan, 2004) to generate the initial NLRP3-ASC and NLRP3-NLRP3 dimer models. The dimer structures were modified at K21/22 positions in Coot before going through the YASARA energy minimization server (Krieger et al., 2009) to produce the final structure models. The interface analyses were performed in PDBePISA server (Krissinel and Henrick, 2007). Structure images were generated using the PyMOL Molecular Graphics System, Version 1.3 Schrödinger, LLC (Delano, 2002).

## QUANTIFICATION AND STATISTICAL ANALYSIS

Mice were randomized to groups and analysis of mice and tissue samples was performed by investigators blinded to the treatment or the genetic background of the animals. Sample size (n) can be found on the bar graphs representing the biological replicates (the number of mice), except for Figure S2, where n represents the technical replicates (the number of images). No statistical methods were used to predetermine sample sizes or test for normal distribution. The number of biological replicates was chosen based on the nature of the experiments and published papers describing similar experiments. Statistical analysis was performed with Student's t test (Excel). Data are presented as means and error bars represent standard errors. In all corresponding figures, \* represents  $p < 0.05$ . \*\* represents  $p < 0.01$ . \*\*\* represents  $p < 0.001$ . ns represents  $p > 0.05$ .

## DATA AND CODE AVAILABILITY

This study did not generate unique datasets or code.